

Infinite time horizon optimal current control of a stepper motor exploiting a finite element model

J. BERNAT¹, S. STEPIEŃ^{1*}, A. STRANZ¹, G. SZYMAŃSKI¹, and J.K. SYKULSKI²

¹ Chair of Computer Engineering, Poznań University of Technology, 3a Piotrowo St., 60-965 Poznań, Poland

² Electronics and Computer Science, University of Southampton, SO17 1BJ, Southampton, United Kingdom

Abstract. An optimal control theory based method is presented aiming at minimizing the energy delivered from source and the power loss in a stepper motor circuit. A linear quadratic current regulator with an infinite time horizon is employed and its appropriateness for this type of a problem explained. With the purpose of improving the accuracy of the control system, the self and mutual inductances of windings are calculated using a finite element model. The numerically computed results are verified experimentally.

Key words: optimal control theory, linear-quadratic problem, finite element method.

1. Introduction

Accurate and precise control of electric motors is an area of active research worldwide. Efforts concentrate on finding solutions which guarantee high immunity of the drive system to external disturbances, such as a changing load, in terms of realizing prescribed trajectories while minimising associated errors in position, velocity or torque [1–4]. The literature coverage in this field is immense, but some specific topics deserve to be mentioned, in particular the optimal control theory [5, 6], sliding control methods [7–8], adaptive control employing neural networks techniques, fuzzy logic and genetic algorithms [1, 9, 10]. Another common objective is to minimise energy losses in conducting motor parts, as well as the energy delivered from the source itself. This can be achieved by determining the optimal phase excitation switching angles, as discussed for example in [11] and [12]. Optimal energy control might also utilise shape and amplitude modulation of the excitation [13–16] or torque control enhancements by current waveform optimisation [1, 17].

One of the best suited approaches to the optimal current control involves using finite element magnetic field modelling (FEM) which enables accurate determination of energy distribution allowing optimal control theory with linear quadratic current regulator to be employed [18, 19]. This is the focus of this paper.

2. A coupled field-circuit model of the motor

In this paper a linear quadratic regulator is assumed to control the reluctance stepper motor. The motor is modelled using the time-stepping finite element technique. The formulation relies on a strong coupling between magnetic field, driving circuitry and mechanical motion equations yielding a complete description of the state of the motor at every time instance during the numerical iterative process [9, 15, 18, 20]. In the field model the eddy current effect in the conducting regions of the

rotor and stator cores is taken into account. The electromagnetic field can be expressed in terms of two state variables: the magnetic vector potential \mathbf{A} and the electric scalar potential V . The well-known Eq. (1) describes the magnetic field due to the winding currents and eddy currents resulting from rotation and transformation of the electromagnetic field

$$\text{curl} \frac{1}{\mu} \text{curl} \mathbf{A} - \sigma \left[\mathbf{v} \times \text{curl} \mathbf{A} - \frac{\partial \mathbf{A}}{\partial t} - \text{grad} V \right] = \mathbf{J}_o. \quad (1)$$

The sum of externally forced currents in the windings is represented by \mathbf{J}_o , μ stands for permeability and σ for conductivity. The term in the square brackets is the induced electric field. The above field description is complemented by an equation preserving current continuity in the conducting regions:

$$\text{div} [\sigma (\mathbf{v} \times \text{curl} \mathbf{A})] - \text{div} \left[\sigma \frac{\partial \mathbf{A}}{\partial t} \right] - \text{div} [\sigma \text{grad} V] = 0. \quad (2)$$

The equation describing the circuit supplying the motor may be written as

$$\frac{d}{dt} \oint_{l_s} \mathbf{A} d\mathbf{l} = u_s - R i_s, \quad (3)$$

where $s=\{1,2,3,4\}$ denotes the phase number, R is the winding resistance of one phase, i_s is the phase current and u_s is the supply voltage.

It is helpful to write Eqs. (1) and (2) in the integral form

$$\begin{aligned} \int_{\Omega} \text{curl} \left(\frac{1}{\mu} \text{curl} \mathbf{A} \right) d\Omega - \int_{\Omega} \sigma (\mathbf{v} \times \text{curl} \mathbf{A}) d\Omega \\ + \int_{\Omega} \sigma \frac{\partial \mathbf{A}}{\partial t} d\Omega + \int_{\Omega} \sigma \text{grad} V d\Omega = \int_{\Omega} \mathbf{J}_o d\Omega, \end{aligned} \quad (4)$$

$$\oint_S \sigma (\mathbf{v} \times \text{curl} \mathbf{A}) d\mathbf{S} - \oint_S \sigma \frac{\partial \mathbf{A}}{\partial t} d\mathbf{S} - \oint_S \sigma \text{grad} V d\mathbf{S} = 0. \quad (5)$$

The above system may be solved iteratively by means of a time stepping technique. To make this possible, field s need to be

*e-mail: slawomir.stepien@put.poznan.pl

spatially discretized [18]. The numerical implementation of the above formulation has been accomplished using the finite element method. It utilizes 27-node, first order, cylindrical elements to discretize the space. The magnetic vector potential in a single element takes the form of linear combination:

$$\mathbf{A} = \sum_{i=1}^{27} N_i \mathbf{A}_i, \quad (6)$$

where N_i are the element shape functions and \mathbf{A}_i are approximations of the potential at elements' nodes. The solution to field Eqs. (1) and (2), i.e. unknown state space variables \mathbf{A} and V , may be calculated by minimising the corresponding energy functional, the method well suited to systems with energy dissipation [15]. The above equations are well known but are shown here for completeness.

The time – space discrete field equations are developed as follows

$$\mathbf{C}\mathbf{A}^{t+\Delta t} + \frac{1}{\Delta t}\mathbf{D}\mathbf{A}^{t+\Delta t} + \mathbf{E}\mathbf{V}^{t+\Delta t} = \frac{1}{\Delta t}\mathbf{D}\mathbf{A}^t + \mathbf{J}^{t+\Delta t}, \quad (7)$$

$$\mathbf{F}\mathbf{A}^{t+\Delta t} - \Delta t\mathbf{H}\mathbf{A}^{t+\Delta t} + \Delta t\mathbf{G}\mathbf{V}^{t+\Delta t} = \mathbf{F}\mathbf{A}^t, \quad (8)$$

where

$$[\mathbf{C}][\mathbf{A}^{t+\Delta t}] \approx \int_{\Omega} \text{curl} \left(\frac{1}{\mu} \text{curl} \mathbf{A}^{t+\Delta t} \right) d\Omega$$

$$- \int_{\Omega} \sigma (\mathbf{v} \times \text{curl} \mathbf{A}^{t+\Delta t}) d\Omega,$$

$$\left[\frac{1}{\Delta t} \mathbf{D} \right] [\mathbf{A}^{t+\Delta t} - \mathbf{A}^t] \approx \int_{\Omega} \sigma \frac{\partial \mathbf{A}}{\partial t} d\Omega$$

$$\approx \int_{\Omega} \sigma \frac{\mathbf{A}^{t+\Delta t} - \mathbf{A}^t}{\Delta t} d\Omega,$$

$$[\mathbf{E}][\mathbf{V}^{t+\Delta t}] \approx \int_{\Omega} \sigma \text{grad} \mathbf{V}^{t+\Delta t} d\Omega,$$

$$[\mathbf{F}][\mathbf{A}^{t+\Delta t} - \mathbf{A}^t] \approx \oint_S \sigma \frac{\partial \mathbf{A}}{\partial t} d\mathbf{S} \approx \oint_S \sigma \frac{\mathbf{A}^{t+\Delta t} - \mathbf{A}^t}{\Delta t} d\mathbf{S},$$

$$[\mathbf{G}][\mathbf{V}^{t+\Delta t}] \approx \oint_S \sigma \text{grad} \mathbf{V}^{t+\Delta t} d\mathbf{S},$$

$$[\mathbf{H}][\mathbf{A}^{t+\Delta t}] \approx \oint_S \sigma (\mathbf{v} \times \text{curl} \mathbf{A}^{t+\Delta t}) d\mathbf{S}.$$

The motor electric circuit equation in discrete notation takes the form

$$\frac{1}{\Delta t} \mathbf{Q}\mathbf{A}^{t+\Delta t} + \mathbf{R}\mathbf{I}^{t+\Delta t} = \mathbf{U}^{t+\Delta t} + \frac{1}{\Delta t} \mathbf{Q}\mathbf{A}^t, \quad (9)$$

where

$$\mathbf{Q}\mathbf{A}^{t+\Delta t} = \left[\oint_{l_1} \mathbf{A} d\mathbf{l} \quad \dots \quad \oint_{l_4} \mathbf{A} d\mathbf{l} \right]^T \quad \text{and} \quad \mathbf{R}$$

represents the diagonal matrix of the windings resistance.

In order to facilitate coupling between the field and circuit equations, the phase current density vector \mathbf{J} can be expressed in terms of a linear combination of the phase current vector \mathbf{I} , yielding $\mathbf{J}^{t+\Delta t} = \mathbf{P}\mathbf{I}^{t+\Delta t}$. Thus the coupled model can be expressed in matrix notation as

$$\begin{bmatrix} \mathbf{C} + \frac{1}{\Delta t} \mathbf{D} & \mathbf{E} & \mathbf{P} \\ \mathbf{F} - \Delta t \mathbf{H} & \Delta t \mathbf{G} & \mathbf{0} \\ \frac{1}{\Delta t} \mathbf{Q} & \mathbf{0} & \mathbf{R} \end{bmatrix} \begin{bmatrix} \mathbf{A}^{t+\Delta t} \\ \mathbf{V}^{t+\Delta t} \\ \mathbf{I}^{t+\Delta t} \end{bmatrix} = \begin{bmatrix} \frac{1}{\Delta t} \mathbf{D} & \mathbf{0} & \mathbf{0} \\ \mathbf{F} & \mathbf{0} & \mathbf{0} \\ \frac{1}{\Delta t} \mathbf{Q} & \mathbf{0} & \mathbf{0} \end{bmatrix} \begin{bmatrix} \mathbf{A}^t \\ \mathbf{V}^t \\ \mathbf{I}^t \end{bmatrix} + \begin{bmatrix} \mathbf{0} \\ \mathbf{0} \\ \mathbf{U}^{t+\Delta t} \end{bmatrix}, \quad (10)$$

where \mathbf{A} and \mathbf{V} represent vectors of unknown magnetic and electric potentials at all nodes, respectively, \mathbf{I} is a vector of unknown currents in nodes surrounding the motor windings, submatrices \mathbf{C} , \mathbf{D} , \mathbf{E} , \mathbf{F} , \mathbf{H} , \mathbf{G} have already been defined for Eqs. (7) and (8), while \mathbf{Q} and \mathbf{R} in (9) and \mathbf{P} (10) are matrices related to winding currents.

3. Mechanical motion model

The mechanical motion is a result of an electromagnetic torque acting on the rotor. The force may be derived using the Maxwell stress tensor. To calculate global torque the integration is performed using the eggshell method [9, 18]

$$T_{\text{mag}} = \oint_S (r \cdot P) dS. \quad (11)$$

The motion of the stepper motor is analysed in a cylindrical coordinate system using a well-known second order differential equation

$$J \frac{d^2 \varphi}{dt^2} + b \left| \frac{d\varphi}{dt} \right| \frac{d\varphi}{dt} = T_{\text{mag}}, \quad (12)$$

where J is the inertia, b the friction coefficient, winding currents.

T_{mag} the electromagnetic torque and φ the angular displacement. Applying time discretization using Euler's method the following system of equation results

$$\begin{bmatrix} 1 & -\Delta t \\ 0 & 1 + \Delta t \frac{b}{J} \end{bmatrix} \begin{bmatrix} \varphi^{t+\Delta t} \\ \omega^{t+\Delta t} \end{bmatrix} = \begin{bmatrix} \varphi^t \\ \omega^t + \frac{\Delta t}{J} T_{\text{mag}}^{t+\Delta t} \end{bmatrix}, \quad (13)$$

where ω denotes angular velocity.

Using an iterative method the rotor displacement is calculated at each time step and then transformed into discretized space using the fixed grid technique, independent of rotor position. It is essential that space discretization creates equidistant nodes in the direction of movement to preserve constant mass of the moving body. Furthermore, the time axis needs to be discretized in a way which guarantees single step rotor

movements not to exceed the distance between neighbouring space nodes. An online method for time step correction ensures this condition is fulfilled at each iteration. This approach prevents stability loss during the solution of the field-circuit Eq. (10).

4. Linear quadratic optimal control

The optimal control theory focuses on optimising a control law which transfers a dynamic system from some initial to some terminal state, by putting on the control law a requirement to extremize an objective functional associated with this system. The form of an objective functional depends on the class of problem. For minimisation of energy in the drive circuit, a linear quadratic performance index is a reasonable solution. It helps finding optimal waveforms of voltage excitation supplied to motor coils in terms of minimisation of energy delivered and power losses in windings resistance [9, 11, 15, 18, 19, 21]. The assumed performance index for control in infinite time horizon takes the following form

$$J(\mathbf{U}) = \frac{1}{2} \int_0^{\infty} (\mathbf{I}^T \mathbf{Q}_J \mathbf{I} + \mathbf{U}^T \mathbf{P}_J \mathbf{U}) dt, \quad (14)$$

subject to the initial state $\mathbf{I}(0) = [i_1(0) \ \dots \ i_n(0)]^T$ and the electric system described as

$$\mathbf{L} \frac{d}{dt} \mathbf{I} + \mathbf{R} \mathbf{I} = \mathbf{U}, \quad (15)$$

where \mathbf{U} , a vector of voltages applied to motor windings, is the unknown optimal solution minimising the functional, \mathbf{I} , a vector of windings currents, is the system state vector, \mathbf{Q}_J and \mathbf{P}_J denote positive definite matrices containing weighting factors, \mathbf{L} is a matrix of unsteady self and mutual winding inductances, and \mathbf{R} is a diagonal matrix of winding resistances. In Eq. (14) the first integrated quadratic form corresponds to power dissipated in windings, the second one to power delivered from the current source.

Due to unsteadiness the coefficients of matrix \mathbf{L} need to be calculated every time step

$$\mathbf{L} = \begin{bmatrix} \frac{\Phi_1}{i_1} & \frac{\Phi_1}{i_2} & \dots & \frac{\Phi_1}{i_n} \\ \frac{\Phi_2}{i_1} & \frac{\Phi_2}{i_2} & \dots & \frac{\Phi_2}{i_n} \\ \vdots & \vdots & \ddots & \vdots \\ \frac{\Phi_n}{i_1} & \frac{\Phi_n}{i_2} & \dots & \frac{\Phi_n}{i_n} \end{bmatrix}. \quad (16)$$

Inductances depend on the magnetic flux penetrating the coils and can be expressed via magnetic potential \mathbf{A} as $\Phi_k = z \oint_{l_k} \mathbf{A} d\mathbf{l}$, where z is the number of turns and l_k denotes the length of a winding.

To find an optimal solution, \mathbf{U}^* , the Pontryagin's Minimum Principle is employed, first introducing the Hamiltonian defined as

$$H(\mathbf{U}, \mathbf{I}, \boldsymbol{\Psi}) = \frac{1}{2} (\mathbf{I}^T \mathbf{Q}_J \mathbf{I} + \mathbf{U}^T \mathbf{P}_J \mathbf{U}) + \boldsymbol{\Psi}^T (\mathbf{L}^{-1} \mathbf{U} - \mathbf{L}^{-1} \mathbf{R} \mathbf{I}), \quad (17)$$

where $\mathbf{L}^{-1} \mathbf{U} - \mathbf{L}^{-1} \mathbf{R} \mathbf{I}$ is the state equation and $\boldsymbol{\Psi}$ is the co-state and may be expressed as $\boldsymbol{\Psi} = \boldsymbol{\Gamma} \mathbf{I}$, where $\boldsymbol{\Gamma}$ is a matrix of time invariant feedback coefficients.

For \mathbf{U}^* to minimize the Hamiltonian, it must satisfy the condition $\frac{\partial H}{\partial \mathbf{U}} = \mathbf{0}$, hence

$$\mathbf{U}^* = -\mathbf{P}_J^{-1} \mathbf{L}^{-1} \boldsymbol{\Psi}. \quad (18)$$

Based on Pontryagin's theory, $\boldsymbol{\Psi}$ and \mathbf{I} are related through the equation

$$\frac{d\boldsymbol{\Psi}}{dt} = -\frac{\partial H}{\partial \mathbf{I}} = (-\mathbf{Q}_J + \mathbf{L}^{-1} \mathbf{R} \boldsymbol{\Gamma}) \mathbf{I}. \quad (19)$$

Furthermore, differentiating $\boldsymbol{\Psi}$ in terms of time gives

$$\frac{d\boldsymbol{\Psi}}{dt} = \boldsymbol{\Gamma} \frac{d\mathbf{I}}{dt} = \boldsymbol{\Gamma} \mathbf{L}^{-1} \mathbf{U}^* - \boldsymbol{\Gamma} \mathbf{L}^{-1} \mathbf{R} \mathbf{I}. \quad (20)$$

Comparing the right hand sides of Eqs. (19) and (20), inserting the optimal control condition (18) and eliminating \mathbf{I} , results in a Riccati equation describing an LQ regulator

$$\boldsymbol{\Gamma} \mathbf{L}^{-1} \mathbf{P}_J^{-1} \mathbf{L}^{-1} \boldsymbol{\Gamma} + \boldsymbol{\Gamma} \mathbf{L}^{-1} \mathbf{R} + \mathbf{L}^{-1} \mathbf{R} \boldsymbol{\Gamma} - \mathbf{Q}_J = \mathbf{0}. \quad (21)$$

The matrix $\boldsymbol{\Gamma}$, obtained after solving the above equation, is then used to derive the optimal control law as a function of \mathbf{I}

$$\mathbf{U}^* = -\mathbf{P}_J^{-1} \mathbf{L}^{-1} \boldsymbol{\Gamma} (\mathbf{I} - \mathbf{N} \mathbf{I}_{\text{ref}}), \quad (22)$$

where the matrix \mathbf{N} is a scaling matrix which enables finding such an optimal control voltage \mathbf{U}^* which guarantees reaching the prescribed current \mathbf{I}_{ref} . The matrix \mathbf{N} is calculated under steady state and equals

$$\mathbf{N} = \boldsymbol{\Gamma}^{-1} \mathbf{L} \mathbf{P}_J \mathbf{R} + \mathbf{Y}, \quad (23)$$

where \mathbf{Y} is an identity matrix.

5. The motor drive and its numerical model

The reluctance stepper motor assumed in this work has 4 phases and 6 rotor poles. The cross section of the motor is presented in Fig. 1. The power controller comprises a PWM generator, delivering the voltage control law calculated by LQR, and a phase switching unit, with its diagram depicted in Fig. 2, enabling the windings to be energized in a unipolar fashion. In addition, the drive is equipped with a Hall sensor based ACS 721 module for winding current measurements and an incremental encoder, with resolution of 400 imp/rev, for rotor displacement feedback.

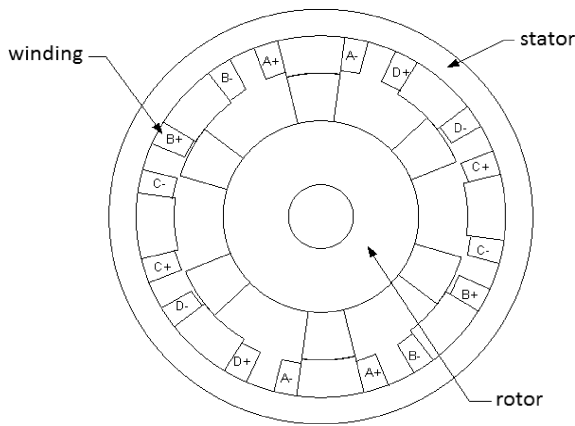


Fig. 1. Stepper motor cross section

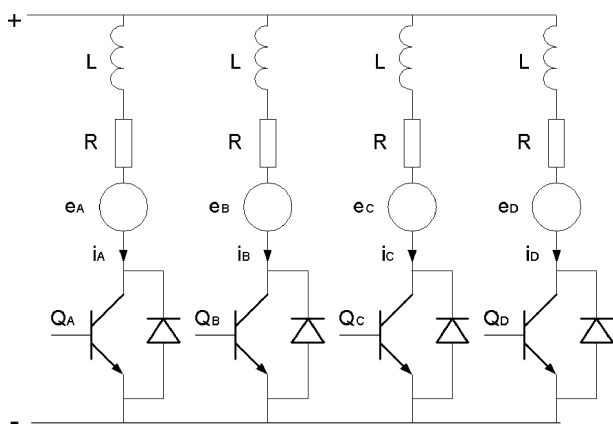


Fig. 2. Phase power switching controller

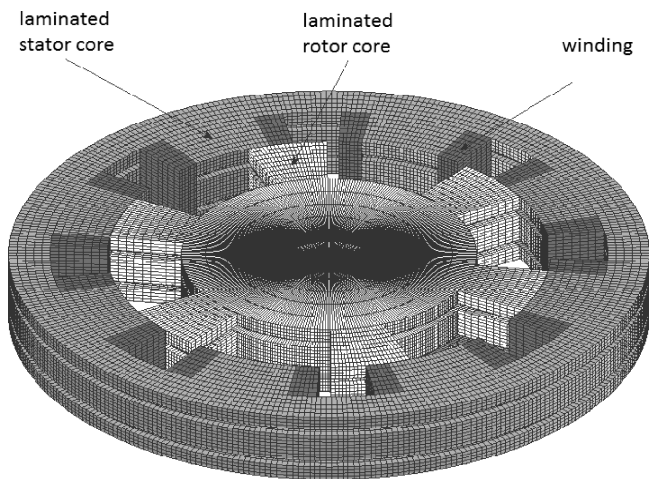


Fig. 3. Discretised model of a stepper motor

The discretised model of a slice of the motor is presented in Fig. 3. Its discretisation grid has 68 926 nodes. The numerical model has 170 640 unknown variables, with 55 440 unknown A_r , 50 400 unknown A_ϕ , and 64 800 unknown A_z , that is components of the vector potential. The biconjugate gradients method (BiCG) accuracy is set to 1.0×10^{-5} . The eddy current effect and the nonlinear $B(H)$ relationship for the

silicon steel core of the rotor and stator are both taken into account [15, 18, 20, 22].

6. Numerical and experimental results

The linear quadratic current control applied to the described stepper motor is assumed to minimise the following performance index

$$J(\mathbf{U}) = \frac{1}{2} \int_0^\infty \mathbf{U}^T \mathbf{U} dt, \quad (24)$$

which is a simplified version of (14). Finding the control law \mathbf{U} requires solving the Riccati Eq. (21) to find the matrix $\mathbf{\Gamma}$, whose coefficients are functions of motor mutual and self-inductances. For the reasons of simulation accuracy the inductance values are computed and compared with measurements.

The dependence of the self and mutual inductances on rotor position is shown in Fig. 4, for all motor phases. The values vary in a range of up to one order of magnitude. Figure 5 compares calculated and measured results for one of the phases, demonstrating good agreement, with slight differences due to inevitable simplifications in the FE model of motor windings, where coils are assumed to be symmetrically wound, and eddy current effects inside are neglected.

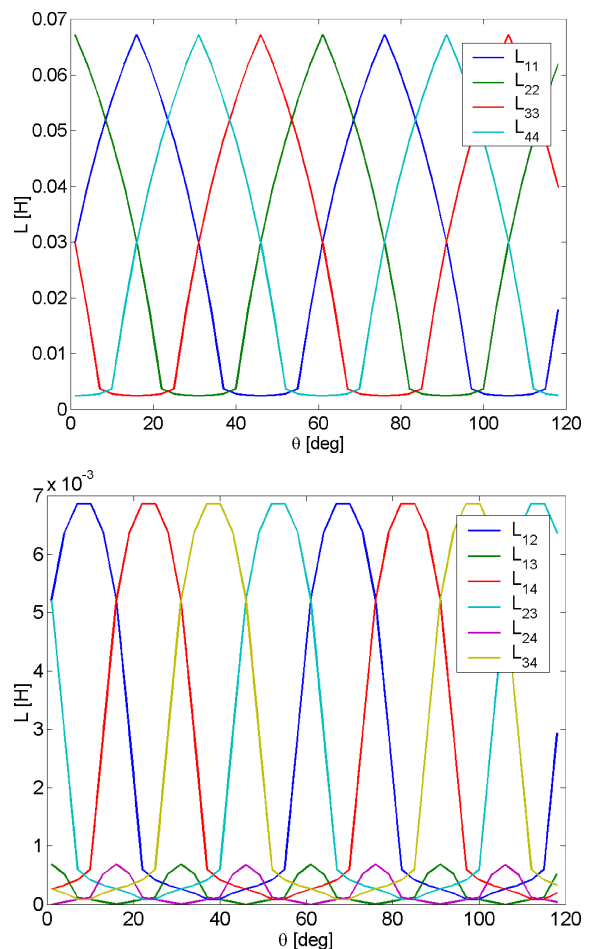


Fig. 4. Phase self-inductance (upper) and mutual inductance (right) as a function of rotor position

Infinite time horizon optimal current control of a stepper motor exploiting a finite element model

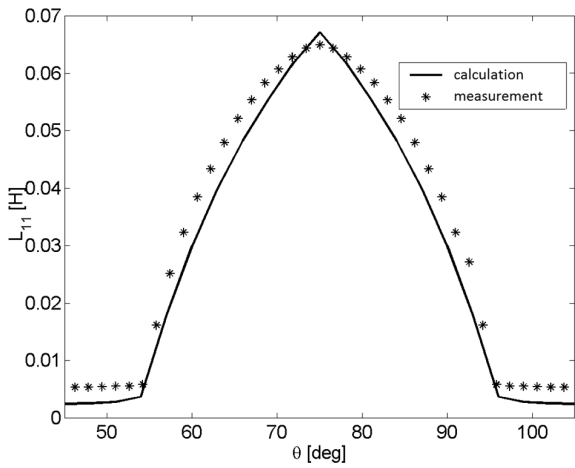


Fig. 5. Comparison between calculated and measured inductance for one phase

Since the inductances are not constant, the coefficients of the matrix Γ , presented in Fig. 6, need to be calculated at every rotor position to ensure sufficient accuracy of the optimal control law

$$U^* = -L^{-1}\Gamma(I - NI_{ref}). \quad (25)$$

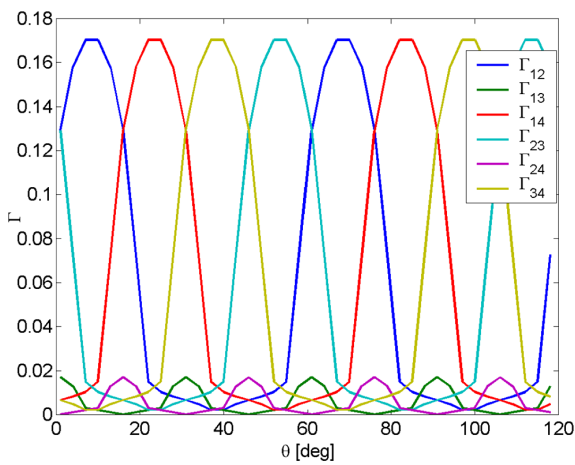
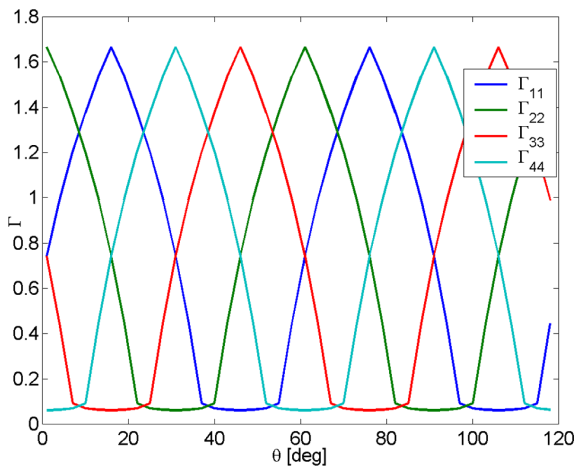


Fig. 6. Matrix Γ coefficients in relation to rotor position

The relevance of the optimal control approach is demonstrated by a numerical calculation assuming I_{ref} to be 1.6 A and the time horizon of 100 ms. Figure 7 depicts the voltage excitation applied by the LQR, with current in the first phase, while Fig. 8 shows the rotor displacement.

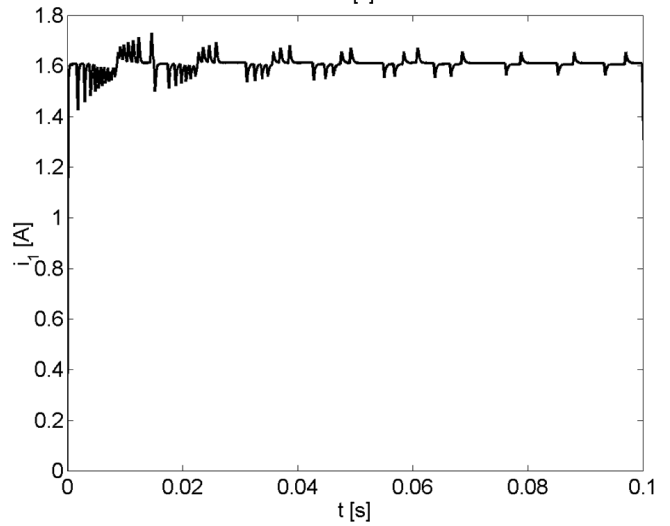
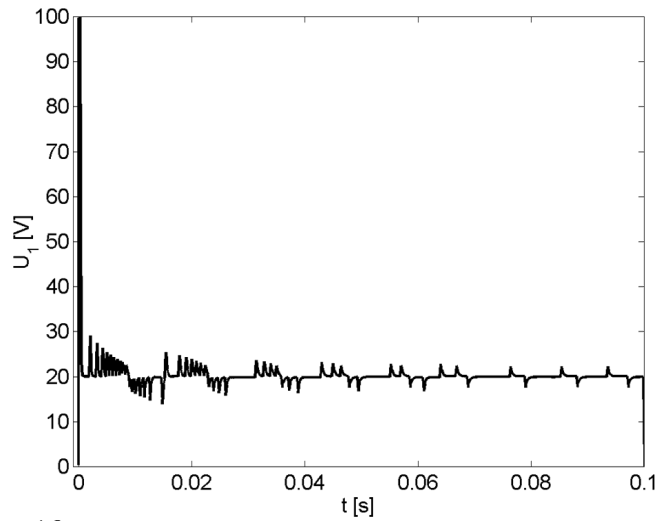


Fig. 7. Voltage excitation and current in phase #1 for $I_{ref} = 1.6$ A

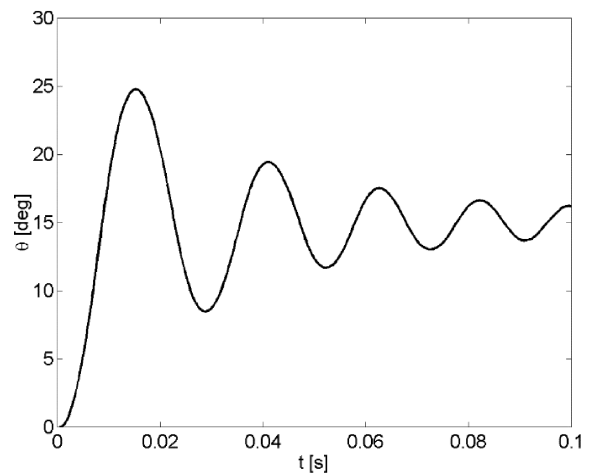


Fig. 8. Rotor displacement for one phase excitation

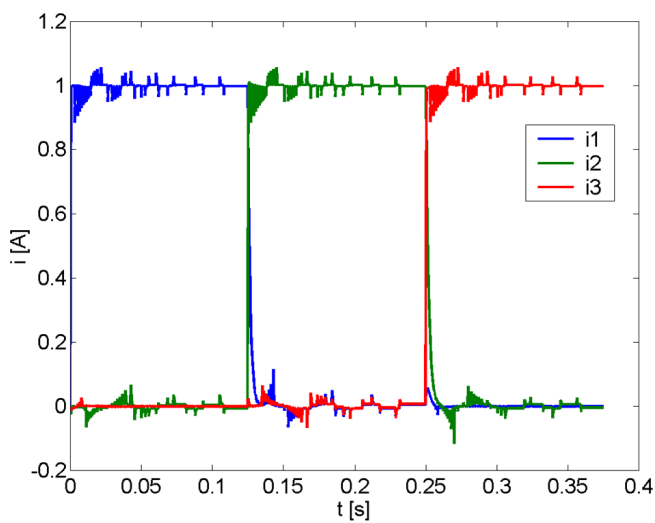
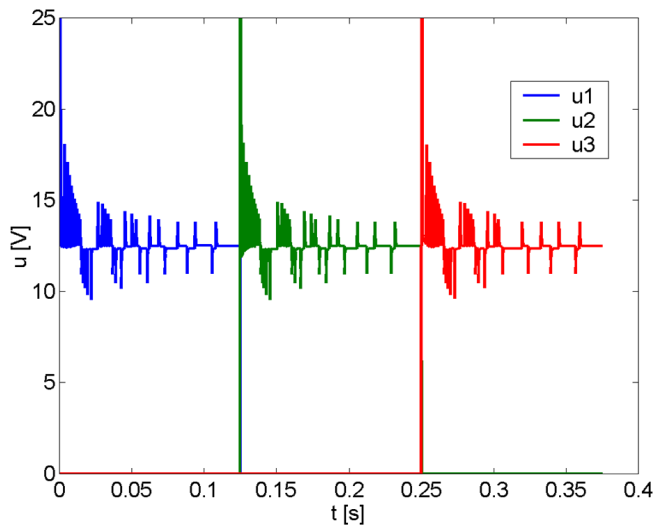


Fig. 9. Voltage excitation and current in phases 1, 2 and 3 for $I_{ref} = 1$ A

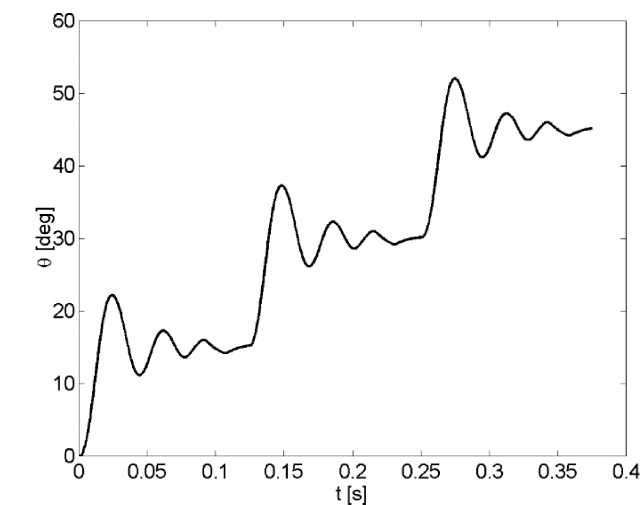


Fig. 10. Rotor displacement for sequence excitation of all three phases

The LQR tries to reach the reference current in the shortest possible time, here in approximately 2 ms, thus the applied voltage rises instantly to 100 V and then abruptly falls down to 20 V. This, obviously, results in higher overshoot in motor position response.

For the sake of practical implementation, the voltage was limited to 25V and the reference current lowered to 1 A. The time horizon for a single phase excitation was increased to 125 ms and three phase switching was performed, which gives 3 rotor steps, hence 45° of angular displacement. Figures 9 and 10 present the voltage sequence excitation for all three phases with their associated currents and motor displacements.

The numerical computation was confronted with an experiment; Figs. 11 and 12 show the measurements of the winding currents and rotor position, respectively.

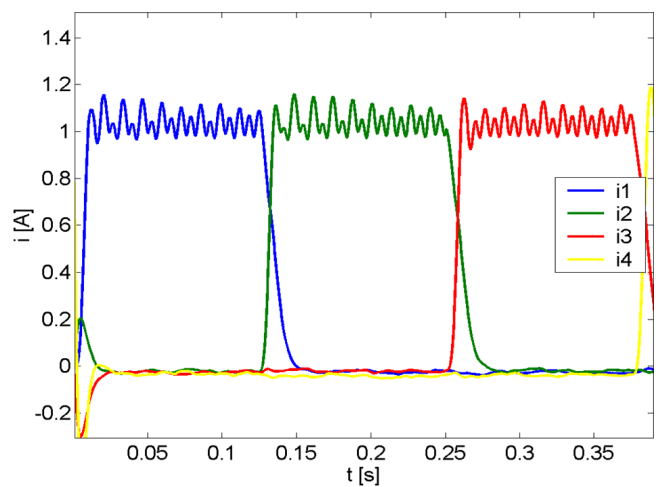


Fig. 11. Measured current in all three phases for $I_{ref} = 1$ A

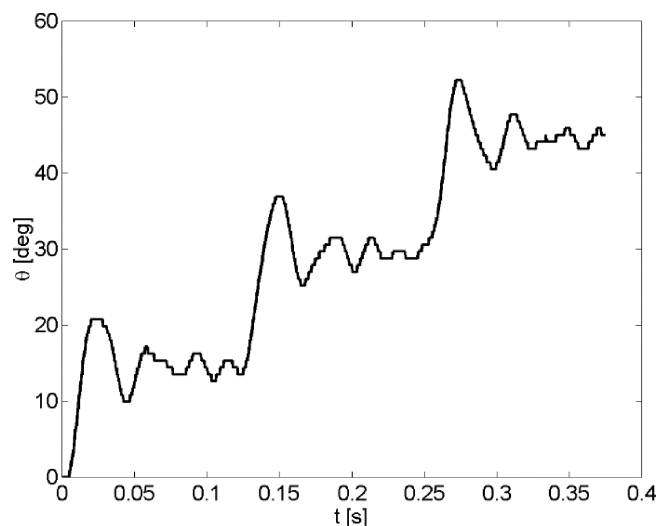


Fig. 12. Measured rotor displacement for sequence excitation of all three phases

Numerical and experimental results compare well in terms of amplitudes, rising times and over-shootings. There are, however, oscillations in the current waveforms, but these can

be attributed to an aftermath of the utilised measuring technique. As far as position measurement is concerned, there are vibrations in the end phase of position settling. This needs to be dealt with by the encoder-motor coupling damping capabilities and encoder resolution itself.

7. Conclusions

In this paper the optimal current control in an infinite time horizon is discussed, and its applicability to the drive energy consumption minimisation presented. The theory is verified by a practical example of a stepper motor control system exploiting a finite element numerical model for inductance calculations. The numerical results exhibit effectiveness of the current optimal control. The calculations are compared with experimental results and show very satisfactory agreement.

The effort will continue with focus on further research in the area of optimal control, especially control in finite and infinite time horizons of winding currents, rotor displacement and electromagnetic torque, but also the minimisation of the control errors themselves.

REFERENCES

- [1] F. Aghili, "Adaptive reshaping of excitation currents for accurate torque control of brushless motors", *IEEE Trans. on Control Systems Technology* 36 (5), 356–365 (2008).
- [2] S. Brock, "Sliding mode control of a permanent magnet direct drive under non-linear friction", *COMPEL: Int. J. Computation and Mathematics in Electrical and Electronic Engineering* 30 (3), 853–863 (2011).
- [3] V.M. Hernández-Guzmána and R.V. Carrillo-Serranoa, "Global PID position control of PM stepper motors and PM synchronous motors", *Int. J. Control* 84 (11), 1807–1816 (2011).
- [4] V.M. Hernández-Guzmána, R.V. Carrillo-Serranoa, and R. Silva-Ortigoza, "PD control for robot manipulators actuated by switched reluctance motors", *Int. J. Control* 86 (3), 540–554 (2013).
- [5] D.E. Miller and M. Rossi, "Simultaneous stabilization with near optimal LQR performance", *IEEE Trans. on Automatic Control* 46 (10), 1543–1555 (2001).
- [6] T. Kaczorek, "Necessary and sufficient conditions for the minimum energy control of positive discrete-time linear systems with bounded inputs", *Bull. Pol. Ac.: Tech.* 62 (1), 85–89 (2014).
- [7] M. Defoort, T. Floquet, A. Kokosy, and W. Perruquetti, "A novel higher order sliding mode control scheme", *System and Control Letters* 58 (2), 102–108 (2009).
- [8] S. Laghrouche, F. Plestan, and A. Glumineau, "Higher order sliding mode control based on integral sliding mode", *Automatica* 43 (3), 531–538.
- [9] S. Stępień, J. Bernat, and G. Szymański, "Fuzzy logic optimal control of BLDC motor considering LQR and SMC methodology", *Foundation of Computing and Decision Science* 35 (3), 171–173 (2010).
- [10] S. Mir, M.S. Islam, T. Sebastian, and I. Husain, "Fault-tolerant switched reluctance motor drive using adaptive fuzzy logic controller", *IEEE Trans. Power Electron.* 19 (2), 289–295 (2004).
- [11] S.H. Mao and M.C. Tsai, "An analysis of the optimum operating point for a switched reluctance motor", *J. Magnetism and Magnetic Materials* 282, 53–56 (2004).
- [12] Z. Cheng, N. Takahashi, B. Forghani, G. Gilbert, Y. Du, Y. Fan, L. Liu, Z. Zhai, W. Wu, and J. Zhang, "Effect of excitation patterns on both iron loss and flux in solid and laminated steel configurations", *IEEE Trans. Magn.* 46 (8), 3185–3188 (2010).
- [13] J.W. Kimball, P.T. Krein, and Y. Chen, "Hysteresis and delta modulation control of converters using sensorless current mode", *IEEE Trans. Power Electron.* 21 (4), 1154–1158 (2006).
- [14] Y. Sozer, D.A. Torrey, and E. Mese, "Automatic control of excitation parameters for switched-reluctance motor drives", *IEEE Trans. on Power Electron.* 18 (2), 594–603 (2003).
- [15] J. Bernat and S. Stępień, "Minimum energy control analysis of the switched reluctance stepper motor considering a nonlinear finite element model", *Simulation Modelling Practice and Theory* 28 (1), 1–11 (2012).
- [16] K. Dębowski, "Determination of optimal current in the non-ideal one-phase system with unsteady parameters", *Bull. Pol. Ac.: Tech.* 62 (2), 387–391 (2014).
- [17] G.H. Jang and C.J. Lee, "Design and control of the phase current of a brushless dc motor to eliminate cogging torque", *J. Applied Physics* 99 (8), 395–403 (2006).
- [18] J. Bernat and S. Stępień, "Modeling and optimal control of variable reluctance stepper motor", *COMPEL: Int. J. Computation and Mathematics in Electrical and Electronic Engineering* 30 (2), 726–740 (2011).
- [19] P. Ignaciuk and A. Bartoszewicz, "Linear-quadratic optimal control of periodic-review perishable inventory systems", *IEEE Trans. on Control Systems Technology* 99, 1–8 (2011).
- [20] K. Vijayakumar, R. Karthikeyan, S. Paramasivam, R. Arumugam, and K. Srini-vas, "Switched reluctance motor modeling, design, simulation, and analysis: a comprehensive review", *IEEE Trans. Mag.* 44 (12), 4605–4617 (2008).
- [21] H. Allihalli and M.I. Bayindir, "Time-energy optimal control of vector controlled induction motor", *COMPEL: Int. J. Computation and Mathematics in Electrical and Electronic Engineering* 21 (2), 235–251 (2002).
- [22] J. Bernat, J. Kolota, S. Stępień, and J. Sykulski, "A steady state solver for modelling rotating electromechanical devices exploiting the transformation from time to position domain", *Int. J. Numerical Modelling: Electronic Networks, Devices and Fields* 27 (2), 213–228 (2014).